Inorg. Chem. **2008**, *47*, 10895−10905

Neutron Powder Diffraction, Multinuclear, and Multidimensional NMR Structural Investigation of $Pb_5Ga_3F_{19}$

Charlotte Martineau,*[,†,‡] Franck Fayon,[§] Christophe Legein,[†] Jean-Yves Buzaré,[‡] François Goutenoire,[†] and Emmanuelle Suard[||]

Laboratoire des Oxydes et Fluorures, CNRS UMR 6010, Institut de Recherche en Ingénierie Moléculaire et Matériaux Fonctionnels, CNRS FR 2575, Université du Maine, Avenue Olivier Messiaen, 72085 Le Mans Cedex 9, France, Laboratoire de Physique de l'Etat Condensé, CNRS UMR 6087, Institut de Recherche en Ingénierie Moléculaire et Matériaux Fonctionnels, CNRS FR 2575, Université du Maine, Avenue Olivier Messiaen, 72085 Le Mans Cedex 9, France, Conditions Extrêmes et Matériaux: Haute Température et Irradiation, CNRS UPR 3079, 1D Avenue de la Recherche Scientifique, 45071 Orléans Cedex 2, France, Université d'Orléans, Faculté des Sciences, Avenue du Parc Floral, 45067 Orléans Cedex 2, France, and Institut Lauë-Langevin, 6 rue J. Horowitz, BP 156, 38042 Grenoble Cedex 9, France

Received June 9, 2008

The room temperature structure of $Pb_5Ga_3F_{19}$ is investigated by combining neutron diffraction and multinuclear ^{19}F, ^{71}Ga, and ^{207}Pb one-dimensional and two-dimensional solid-state nuclear magnetic resonance (NMR) experiments. Two models built in space group *I*4*cm* are reported for the description of the crystalline structure of $Pb_5Ga_3F_{19}$. The structure is built from a network of both opposite corner-sharing $Ga2F_6^{3-}$ octahedra forming infinite chains along the *c*-axis and isolated $Ga1F_6^{3-}$ octahedra. The two models present two slightly different views of the strong static disorder of the fluorine ions belonging to the $Ga2F_6^{3-}$ octahedra. ^{71}Ga NMR results show that the local environment of all Ga2 ions is identical, which indicates a tilt of the $Ga2F_6^{3-}$ octahedra within the chains. ^{207}Pb NMR experiments confirm that the environment of only one of the two lead sites, Pb1, is strongly affected by the disorder, which gives rise to three broad distinct ^{207}Pb NMR lines for this site. All ^{19}F NMR lines are assigned using the ^{19}F DQ-SQ MAS experiment. $^{19}F-^{207}Pb$ through-bond and through-space heteronuclear correlation experiments are carried out for the first time, supporting assignment of both the ^{19}F and ^{207}Pb NMR spectra. These correlation experiments also show that both models correctly describe the medium-range order of the structure of $Pb_5Ga_3F_{19}$.

Introduction

High-resolution solid-state magic angle spinning (MAS) nuclear magnetic resonance (NMR) has emerged as a complementary method to diffraction techniques for the investigation of crystal structures. The former is more sensitive to local order, as NMR interactions are short-range in character, whereas the latter provides information about the medium-range order. Therefore, the combination of both methods offers substantial advantages for the understanding of the structure of solids.

During the past decade, very important technological advancements (higher magnetic field and very fast MAS spinning frequency) and methodological advancements (pulse sequence design) have greatly improved the resolution of the MAS NMR spectra and also have widened the range of NMR experiments that can be applied to solid materials. Cross-polarization[1,2] (CP) is routinely used in NMR of spin $I = {}^1/_2$ as a mean of enhancing sensitivity by magnetization transfer between dipolar-coupled abundant and diluted nuclei. Therefore, the CP-MAS technique is a valuable spectral editing tool that can be used to determine heteronuclear spatial proximities through CP heteronuclear correlation (CP-HETCOR) experiments.[3] More recently in solids, *J*-coupling

* To whom correspondence should be addressed. E-mail: charlotte.martineau.etu@univ-lemans.fr. Fax: +33243833506.
† Laboratoire des Oxydes et Fluorures, Université du Maine.
‡ Laboratoire de Physique de l'Etat Condensé, Université du Maine.
§ CEMHTI and Université d'Orléans.
|| Institut Lauë-Langevin.

(1) Hartmann, S. R.; Hahn, E. L. *Phys. Rev.* **1962**, *128*, 2042–2053.
(2) Pines, A.; Gibby, M. G.; Waugh, J. S. *J. Chem. Phys.* **1972**, *56*, 1776–1777.

10.1021/ic801044j CCC: $40.75
Published on Web 10/30/2008

also was proven to be an important structural probe because the establishment of through bond connectivities, using experiments like the heteronuclear multiple-quantum correlation (*J*-HMQC)[4] or the heteronuclear simple-quantum correlation (*J*-HSQC[5]) ones, and the corresponding *J*-coupling constant values provide detailed insights into the structure of crystalline or amorphous phases.[6] Homonuclear correlations are also a worthwhile source of structural information, being transmitted through homonuclear *J*-coupling, in experiments like the incredible natural abundance double-quantum transfer experiment (INADEQUATE)[7−9] or the refocused INADEQUATE,[10] or through dipolar coupling in the double-quantum single-quantum (DQ-SQ) correlation experiments.[11]

In inorganic fluorides, two-dimensional (2D) heteronuclear correlation experiments have already been applied to a few spin pairs, $^{19}F/^{27}Al$,[12−25] $^{19}F/^{23}Na$,[20,26−28] and $^{19}F/^{31}P$,[13] to probe heteronuclear spatial proximities; however, obtaining high-resolution ^{19}F MAS NMR spectra usually requires the use of very fast spinning frequencies, which result in a decrease of the magnetization transfer efficiency in the HETCOR experiment and a long experiment time. Recently, we showed the occurrence of particularly strong $^{19}F-^{207}Pb$ *J*-couplings in $Pb_5Ga_3F_{19}$ (ranging from 0.9 to 4.6 kHz),[29] which open the use of heteronuclear correlation methods based on isotropic *J*-coupling.[4,5] In oxyfluorides, $^{19}F-^{19}F$ DQ-SQ MAS correlation experiments were conducted, determining homonuclear fluorine−fluorine proximities.[30] In this context, this ensemble of techniques appears very attractive for characterizing the structure of crystalline or amorphous inorganic fluorides.

$Pb_5Ga_3F_{19}$ is a recrystallization product[31] of the transition metal fluoride glass family $PbF_2-ZnF_2-GaF_3$ (PZG).[32] Heavy metal fluoride glasses are of particular interest for their optical properties.[33] Among them, PZG glass planar waveguides can be prepared by physical vapor deposition.[34] $Pb_5Ga_3F_{19}$ was identified in 1970 as $Pb_3Ga_2F_{12}$ by Grannec et al.[35] who studied the PbF_2-GaF_3 binary system. At the same time, de Kozak reported a related compound identified as $Pb_3Cr_2F_{12}$[36] (PDF[37] file number 00-023-0346). Later, Ravez et al. showed that this compound was actually $Pb_5Cr_3F_{19}$ (PDF[37] file number 00-047-0286) and published its structure[38] (tetragonal space group (SG) *I*4*cm*), which was resolved from single-crystal X-ray diffraction data (PDF[37] file number 04-007-2802, ICSD[39] file number 66050). $Pb_5Ga_3F_{19}$ and the related compounds $Pb_5M^{III}_3F_{19}$ [M = Al (phase V), Ti, V, and Fe] were then reported to be isostructural with $Pb_5Cr_3F_{19}$.[40] Cell parameters were determined for $Pb_5Ga_3F_{19}$ (PDF[37] file number 00-047-0287, a = 14.361 Å and c = 7.441 Å), but no accurate structural solution was given. However, a structure of $Pb_5Ga_3F_{19}$ calculated in SG *I*4/*m* is reported in the PDF[37] database with file number 04-006-2919. In the $M^{II}_5M^{III}_3F_{19}$ (M^{II} = Ba, Pb, and Sr and M^{III} = Al, Cr, V, and Fe) family (except phases I, III, and IV of $Pb_5Al_3F_{19}$),[41] two kinds of structures are encountered, which crystallize in either the *I*4/*m* or *I*4*cm* SG. The structures are based on isolated and either edge-sharing octahedra forming dimers ($Sr_5Fe_3F_{19}$,[42] $Sr_5Cr_3F_{19}$,[43] $Sr_5V_3F_{19}$,[43] and $Ba_5Fe_3F_{19}$[43]) or corner-sharing $M^{III}F_6^{3-}$

(3) Caravatti, P.; Braunschweiler, L.; Ernst, R. R. *Chem. Phys. Lett.* **1983**, *100*, 305–310.
(4) Lesage, A.; Sakellariou, D.; Steuernegel, S.; Emsley, L. *J. Am. Chem. Soc.* **1998**, *120*, 13194–13201.
(5) Lesage, A.; Emsley, L. *J. Magn. Reson.* **2001**, *148*, 449–454.
(6) Varaa, J.; Jokisaari, J.; Wasylishen, R. E.; Bryce, D. L. *Prog. Nucl. Magn. Reson. Spectrosc.* **2002**, *41*, 233–304.
(7) Bax, A.; Freeman, R.; Frenkiel, T. A. *J. Am. Chem. Soc.* **1981**, *103*, 2102–2104.
(8) Fyfe, C. A.; Feng, Y.; Gies, H.; Grondey, H.; Kokotailo, G. T. *J. Am. Chem. Soc.* **1990**, *112*, 3264–3270.
(9) Lesage, A.; Auger, C.; Caldarelli, S.; Emsley, L. *J. Am. Chem. Soc.* **1997**, *119*, 7867–7868.
(10) Lesage, A.; Bardet, M.; Emsley, L. *J. Am. Chem. Soc.* **1999**, *121*, 10987–10993.
(11) Jeremy, H. G.; Titman, J. J.; Gottwald, J.; Spiess, H. W. *Chem. Phys. Lett.* **1994**, *227*, 79–86.
(12) Pruski, M.; Lang, D. P.; Fernandez, C.; Amoureux, J. P. *Solid State Nucl. Magn. Reson.* **1997**, *7*, 327–331.
(13) Taulelle, F.; Pruski, M.; Amoureux, J. P.; Lang, D. P.; Bailly, A.; Huguenard, C.; Haouas, M.; Gerardin, C.; Loiseau, T.; Férey, G. *J. Am. Chem. Soc.* **1999**, *121*, 12148–12153.
(14) Fischer, L.; Harlé, V.; Kasztelan, S.; d'Espinose de la Caillerie, J.-B. *Solid State Nucl. Magn. Reson.* **2000**, *16*, 85–91.
(15) Chan, J. C. C.; Eckert, H. *J. Non-Cryst. Solids* **2001**, *284*, 16–21.
(16) Sanchez, N. A.; Saniger, J. M.; d'Espinose de la Caillerie, J.-B.; Blumerfeld, A. L.; Fripiat, J. J. *Microporous Mesoporous Mater.* **2001**, *50*, 41–52.
(17) Taulelle, F. *Solid State Sci.* **2001**, *3*, 795–800.
(18) Fechtelkord, M.; Behrens, H.; Holtz, F.; Bretherton, J. L.; Fyfe, C. A.; Groat, L. A.; Raudsepp, M. *Am. Mineral.* **2003**, *88*, 1046–1054.
(19) Chupas, P. J.; Corbin, D. R.; Rao, V. N. M.; Hanson, J. C.; Grey, C. P. *J. Phys. Chem. B* **2003**, *107*, 8327–8336.
(20) Dutour, J.; Guillou, N.; Huguenard, C.; Taulelle, F.; Mellot-Draznieks, C.; Férey, G. *Solid State Sci.* **2004**, *6*, 1059–1067.
(21) Chupas, P. J.; Grey, C. P. *J. Catal.* **2004**, *224*, 69–79.
(22) Kao, H. M.; Chang, P.-C. *J. Phys. Chem. B* **2006**, *110*, 19104–19107.
(23) Kao, H. M.; Liao, Y. C. *J. Phys. Chem. C* **2007**, *111*, 4495–4498.
(24) Zhang, L.; de Araujo, C. C.; Eckert, H. *J. Phys. Chem. B* **2007**, *111*, 10402–10412.
(25) Amoureux, J. P.; Trébosc, J.; Tricot, G. *Magn. Reson. Chem.* **2007**, *45*, 187–191.
(26) Lim, K. H.; Grey, C. P. *Chem. Phys. Lett.* **1999**, *312*, 45–56.
(27) Lim, K. H.; Grey, C. P. *J. Chem. Phys.* **2000**, *112*, 7490–7504.
(28) Du, L.-S.; Samoson, A.; Tuherm, T.; Grey, C. P. *Chem. Mater.* **2000**, *12*, 3611–3616.
(29) Martineau, C.; Fayon, F.; Legein, C.; Buzaré, J.-Y.; Silly, G.; Massiot, D. *Chem. Commun.* **2007**, 2720–2722.
(30) Alam, T. M.; Clawson, J. S.; Bonhomme, F.; Thomas, S. G.; Rodriguez, M. A.; Zheng, S.; Autschbach, J. *Chem. Mater.* **2008**, *20*, 2205–2217.
(31) Legein, C.; Buzaré, J.-Y.; Jacoboni, C. *J. Solid State Chem.* **1996**, *121*, 149–157.
(32) Miranday, J.-P.; Jacoboni, C.; de Pape, R. *J. Non-Cryst. Solids* **1980**, *43*, 393–401.
(33) Nakajima, T.; Tressaud, A.; Zemva, B. *Advanced Inorganic Fluorides: Synthesis, Characterization and Applications*; Elsevier: Switzerland, 2000.
(34) Jacoboni, C.; Perrot, O.; Boulard, B. *J. Non-Cryst. Solids* **1995**, *184*, 184–189.
(35) Grannec, J.; Ravez, J. *Bull. Soc. Chim. Fr.* **1970**, *5*, 1753–1754.
(36) De Kozak, A. C. R. *Acad. Sci. Ser. C* **1970**, *270*, 949–951.
(37) PDF-4+2007; The International Centre for Diffraction Data (ICDD): Newtown Square, PA, 2007.
(38) Abrahams, S. C.; Albertsson, J.; Svensson, C.; Ravez, J. *Acta Crystallogr.* **1990**, *B46*, 497–502.
(39) Inorganic Crystal Structure Database (ICSD), version 1.4.2; FIZ Karlsruhe and NIST: Germany and Maryland, 2007.
(40) Ravez, J.; Riamampianina, V.; Simon, A.; Grannec, J. *J. Appl. Phys.* **1991**, *70*, 1331–1336.
(41) Abrahams, S. C.; Ravez, J.; Ritter, H.; Ihringer, J. *Acta Crystallogr.* **2003**, *B59*, 557–574.
(42) Graulich, J.; Babel, D. *Z. Anorg. Allg. Chem.* **1991**, *597*, 51–59.
(43) Dahlke, P.; Graulich, J.; Welsh, M.; Pebler, J.; Babel, D. *Z. Anorg. Allg. Chem.* **2000**, *626*, 1255–1263.
(44) Sarraute, S.; Ravez, J. *Acta Crystallogr.* **1995**, *C51*, 1731–1732.

octahedra forming infinite chains along the *c*-axis ($Pb_5Cr_3F_{19}$,[38] phases II[44] and V[45] of $Pb_5Al_3F_{19}$, $Ba_5Mn_3F_{19}$,[43] and $Ba_5Ga_3F_{19}$[43]). Most of the cited compounds present a strong disorder of the fluorine, belonging to the non-isolated $M^{III}F_6^{3-}$ octahedra, which is shown either by large atomic anisotropic displacement parameters (ADPs) of those fluorine ions in $Pb_5Cr_3F_{19}$ or by a statistic distribution of those fluorine ions on particular crystallographic sites ($Sr_5Fe_3F_{19}$, $Sr_5Cr_3F_{19}$, $Sr_5V_3F_{19}$, $Ba_5Mn_3F_{19}$, $Ba_5Fe_3F_{19}$, and $Ba_5Ga_3F_{19}$). In $Ba_5M^{III}_3F_{19}$ compounds, the Ba sites are also distributed.

Because of the difficulties of determining the structure of compounds presenting both light elements (such as fluorine) and heavy elements (such as lead) from X-ray powder diffraction data, we carried out neutron powder diffraction (NPD) experiments. Neutron diffraction is particularly well-adapted for the study of $Pb_5Ga_3F_{19}$ as the coherent scattering lengths of Pb, Ga, and F are on the same order of magnitude (0.9405×10^{-12}, 0.7288×10^{-12}, and 0.5654×10^{-12} cm, respectively).

In this work, we report an investigation of the room temperature structure of $Pb_5Ga_3F_{19}$ by combining neutron diffraction and multinuclear one-dimensional (1D) and 2D NMR experiments. In the late 1990s, Bureau et al. studied $Pb_5Ga_3F_{19}$ (erroneously named $Pb_3Ga_2F_{12}$ in the articles) by ^{19}F, ^{207}Pb, and $^{69,71}Ga$ solid-state 1D NMR.[46−48] However, considering the NMR experimental improvements since then, we report a reinvestigation of the 1D experiments. In addition, the 2D ^{19}F DQ-SQ MAS correlation experiment is performed to determine through-space $^{19}F-^{19}F$ proximities, and the first solid-state through-bond *J*-HMQC spectrum between ^{19}F and another nucleus (^{207}Pb) is shown.

Materials and Methods

1. Synthesis. Usually, 1 g of $Pb_5Ga_3F_{19}$ is synthesized from a solid-state reaction of a stoichiometric mixture of PbF_2 and GaF_3 in sealed platinum tubes (3 mm diameter, 40 mm height). Because these starting materials are moisture sensitive, all operations of weighing, mixing, and grinding were done in a dry glovebox under a nitrogen atmosphere. The mixture was heated at 520 °C for 6 days and naturally cooled. The purity of the obtained phase was checked by the X-ray powder diffraction method against PDF[37] file number 00-047-0287.

2. Neutron Diffraction. The room temperature NPD pattern of $Pb_5Ga_3F_{19}$ was collected on the D2B high-resolution/high-flux powder diffractometer at the Institut Lauë-Langevin in Grenoble, France. It was recorded at $\lambda = 1.5960$ Å for 2 h. Data were acquired at 2θ intevals of 0.05° throughout the angular range $10° < 2\theta < 160°$. The sample was packed in a vanadium can. The Rietveld[49] method using the Fullprof[50] program was used for the structural refinement.

3. NMR Experiments. All ^{19}F and ^{207}Pb 1D and 2D NMR spectra were recorded on an Avance 300 Bruker spectrometer (magnetic field of 7 T) operating at Larmor frequencies of 282.2 and 62.4 MHz for ^{19}F and ^{207}Pb, respectively, using a ^{19}F-optimized CP-MAS probe with a 2.5 mm rotor (spinning frequency up to 35 kHz). A ^{19}F Hahn echo spectrum was acquired at a spinning frequency of 30 kHz using a 2.5 μs 90° pulse (nutation frequency of 100 kHz) and an interpulse delay synchronized with the rotor period. The recycle delays were taken to 1 s. ^{207}Pb continuous wave decoupling (nutation frequency of 70 kHz) was applied during acquisition. The $^{19}F-^{207}Pb$ CP-MAS (20 and 25 kHz) spectra were recorded using a 3 ms contact time, a 1 s recycle delay (relaxation monitored by the ^{19}F T_1 relaxation time), and a ^{19}F continuous wave decoupling (nutation frequency of 40 kHz) during acquisition. ^{207}Pb resonances are particularly broad. Thus, to avoid baseline distortion, the spin-lock was followed by a rotor-synchronized Hahn echo sequence. The processing of the ^{207}Pb CP-MAS spectra was then carried out so that the Fourier transforms started at $t = 0$.[51] The $^{19}F-^{207}Pb$ MAS (20 and 25 kHz) refocused insensitive nuclei enhanced by polarization transfer (*J*-INEPT)[52] spectra were recorded using heteronuclear coherence excitation−reconversion delays of 50−100 μs. The 2D DQ-SQ ^{19}F MAS NMR correlation experiment used an offset compensated back-to-back (BABA) multiple-pulse train sequence for excitation and reconversion of the multiple-quantum coherence.[53] This 2D DQ-SQ MAS NMR correlation experiment used 80 rotor-synchronized t_1 increments, a spinning rate of 30 kHz, and a 2.5 μs 90° pulse length. The DQ excitation and reconversion blocks were set to 66.66 μs, corresponding to two rotor periods. Phase sensitive detection in the $F1$ dimension was obtained using the States method.[54] The $^{19}F-^{207}Pb$ MAS *J*-HMQC spectrum was recorded at a 25 kHz spinning rate. The delays, τ, were synchronized with the rotor period and set to 150 μs. 180 t_1 increments with 80 transients each were accumulated, with a recycle delay of 1 s (corresponding to a total experiment time of 4 h) and continuous wave ^{207}Pb decoupling during acquisition (nutation frequency of 70 kHz). The 2D MAS (25 kHz) $^{19}F-^{207}Pb$ CP-HETCOR spectrum was recorded using the CP conditions mentioned previously. 84 t_1 increments with 3072 transients each were accumulated in the CP-HETCOR (corresponding to a total experiment time of 3 days). A continuous wave ^{207}Pb decoupling (nutation frequency of 70 kHz) was applied during the t_1 period (indirect ^{19}F dimension), as heteronuclear *J*-couplings are not refocused in the CP-HETCOR experiment. We noticed that the ^{19}F and ^{207}Pb spectra of $Pb_5Ga_3F_{19}$ are significantly temperature dependent. Thus, for all MAS experiments, the sample temperature was monitored to 0 °C using an X-trem Bruker cooling unit. The ^{207}Pb isotropic chemical shift of $Pb(NO_3)_2$ was used as an internal NMR thermometer.[55,56] High-field ^{71}Ga static and MAS (14 kHz) Hahn echo NMR spectra were recorded on an Avance 750 Bruker spectrometer (17.6 T) operating at a ^{71}Ga Larmor frequency of 228.77 MHz, using a CP-MAS probe with a 4 mm rotor. Owing to the large quadrupolar broadening of one of the gallium sites, the ^{71}Ga ($I = 3/2$, natural abundance 39.60%) static spectrum extends over a wide frequency range (>9000 kHz). Therefore, short pulse

(45) Sarraute, S.; Ravez, J.; Von Der Mühll, R.; Bravic, G.; Feigelson, R. S.; Abrahams, S. C. *Acta Crystallogr.* **1996**, *B52*, 72–77.
(46) Bureau, B.; Silly, G.; Buzaré, J.-Y.; Emery, J.; Legein, C.; Jacoboni, C. *J. Phys.: Condens. Matter* **1997**, *9*, 6719–6736.
(47) Bureau, B.; Silly, G.; Buzaré, J.-Y. *Solid State Nucl. Magn. Reson.* **1999**, *15*, 79–89.
(48) Bureau, B.; Silly, G.; Buzaré, J.-Y.; Legein, C.; Massiot, D. *Solid State Nucl. Magn. Reson.* **1999**, *14*, 181–190.
(49) Rietveld, H. M. *J. Appl. Crystallogr.* **1969**, *2*, 65–71.
(50) Rodriguez-Carvajal, J. *FULLPROF Program, Rietveld Pattern Matching Analysis of Powder Patterns*; ILL: Grenoble, France, 1990.
(51) Fayon, F.; Farnan, I.; Bessada, C.; Coutures, J.; Massiot, D.; Coutures, J.-P. *J. Am. Chem. Soc.* **1997**, *119*, 6837–6843.
(52) Burum, D. P.; Ernst, R. R. *J. Magn. Reson.* **1980**, *39*, 163–168.
(53) Feike, M.; Demco, D. E.; Graf, R.; Gottwald, J.; Hafner, S.; Spiess, H. W. *J. Magn. Reson.* **1996**, *122*, 214–221.
(54) States, D.; Haberkorn, R.; Ruben, D. *J. Magn. Reson.* **1982**, *48*, 286–292.
(55) Van Gorkom, L. C. M.; Hook, J. M.; Logan, M. B.; Hanna, J. V.; Wasylishen, R. E. *Magn. Reson. Chem.* **1995**, *33*, 791–795.
(56) Bielecki, A.; Burum, D. P. *J. Magn. Reson., Ser. A* **1995**, *116*, 215–220.

Table 1. Atom Label, Wyckoff Multiplicity, Occupancy, Site Symmetry, and Atomic Positions (x, y, z)[a] for Model 1 and Model 2 (in italics) of $Pb_5Ga_3F_{19}$[b]

atom label	Wyckoff multiplicity	occupancy	site symmetry	x	y	z
Ga1	8*c*	1	m	0.1630(2)	0.3370(2)	0.977(1)
		1		*0.1628(2)*	*0.3372(2)*	*0.977(1)*
Ga2	4*a*	1	4	0	0	0.171(1)
		1		*0*	*0*	*0.170(1)*
Pb1	16*d*	1	1	0.4284(2)	0.2719(2)	0
		1		*0.4286(2)*	*0.2719(2)*	*0*
Pb2	4*b*	1	2 mm	0	$^1/_2$	0.144(1)
		1		*0*	$^1/_2$	*0.143(1)*
F1	16*d*	1	1	0.1069(2)	0.2472(4)	0.821(1)
		1		*0.1071(3)*	*0.2478(4)*	*0.823(1)*
F2	16*d*	1	1	0.1988(3)	0.4300(3)	0.151(1)
		1		*0.1989(3)*	*0.4302(3)*	*0.152(1)*
F3	4*a*	1	4	0	0	0.408(3)
	16*d*	0.25	1	*0.0038(3)*	*0.0399(8)*	*0.408(3)*
F4	8*c*	1	m	0.2506(3)	0.2494(3)	0.045(1)
		1		*0.2506(3)*	*0.2494(3)*	*0.046(1)*
F5	8*c*	1	m	0.3867(3)	0.1133(3)	0.008(2)
		1		*0.3871(3)*	*0.1129(3)*	*0.009(2)*
F6	8*c*	1	m	0.0756(5)	0.4244(5)	0.895(1)
		1		*0.0758(5)*	*0.4242(5)*	*0.894(1)*
F7	16*d*	1	1	0.1158(3)	0.0555(4)	0.663(1)
	16*d*	0.5		*0.1171(9)*	*0.0566(9)*	*0.622(2)*
F8	16*d*	0.5	1	*0.1160(9)*	*0.0544(9)*	*0.703(2)*

[a] Uncertainties of atomic positions are in parentheses. [b] Cell parameters are $a = 14.3372(3)$ Å and $c = 7.4346(2)$ Å for model 1 and $a = 14.3369(3)$ Å and $c = 7.4344(2)$ Å for model 2. Reliability factors are $R_p = 0.080$, $R_{wp} = 0.085$, $R_{Bragg} = 0.0226$, and $\chi^2 = 3.96$ for model 1 and $R_p = 0.080$, $R_{wp} = 0.086$, $R_{Bragg} = 0.0221$, and $\chi^2 = 3.97$ for model 2. Respectively, 78 and 76 parameters were refined for model 1 and model 2.

durations (1 μs) were used to ensure a complete irradiation. The recycle delays were set to 500 ms. A static ^{71}Ga Hahn echo spectrum also was recorded on an Avance 400 Bruker spectrometer (9.4 T), operating at a Larmor frequency of 122.04 MHz and using identical experimental conditions. ^{19}F, ^{207}Pb, and ^{71}Ga chemical shifts were referenced to $CFCl_3$, $Pb(CH_3)_4$, and a 1 M $Ga(NO_3)_3$ solution, respectively. All 1D NMR spectra were reconstructed using the DMFit[57] software.

Results and Discussion

1. Neutron Diffraction Data. Both the *I*4/*m* and *I*4*cm* SGs were tested, allowing indexation of all the peaks of the NPD diagram of $Pb_5Ga_3F_{19}$. Nonetheless, extra lines are generated by the *I*4/*m* SG, which are not present. Thus, the solution isotructural with $Pb_5Cr_3F_{19}$ (*I*4*cm* SG) was retained. The atomic coordinates of $Pb_5Cr_3F_{19}$[38] were used as the starting data in the Rietveld refinement of the NPD diagram, replacing chromium atoms by gallium atoms. A first model (model 1), refining ADPs,[58] was tested leading to satisfactory reliability factors (Table 1 and Figure 1). As observed in $Pb_5Cr_3F_{19}$,[40] ADPs are particularly large (Supporting Information) for the fluorine ions F3 and F7, belonging to the corner-sharing octahedra. ADPs may represent either atomic motion or possible static displacive disorder. Fourier difference maps were calculated from the structure of $Pb_5Ga_3F_{19}$ (model 1) with zero nuclear-scattering density on the shared F3 atom (Figures 2a, b) and on the unshared F7 atom (Figures 2c, d). For F3, the maps show a square-based parallelepiped shape with the small length along the *c*-axis. For F7, the maps show an ellipsoidal shape with the main axis of the ellipsoid along the *c*-axis. Then, the second model (model 2) was built replacing the large ADPs by static distributions with shared fluorine ions on the general position 16*d* with 0.25 occupancy and the unshared fluorine, F7, split into two sites on the general position 16*d* with 0.5 occupancy, as for $Ba_5Mn_3F_{19}$.[43] The Rietveld refinement of this model, refining ADPs for all atoms except those whose occupancy is less than one (the best result was obtained using isotropic thermal factors equal to 2.4 Å^2 for these fluorine atoms), leads to reliability factors very similar to that obtained using model 1 (Table 1). The cell parameters of the two models are very similar (Table 1) and close to those observed by Ravez et al.[40] The two models are different descriptions of the static disorder of the fluorine ions of the GaF_6^{3-} octahedron chains.

2. Structural Description. Whatever the model, the backbone of the structure of $Pb_5Ga_3F_{19}$ is identical (Figure 3) and involves two 6-fold coordinated gallium ions and one 10-fold (Pb2) coordinated lead ion and one 11-fold (Pb1) coordinated lead ion. In model 1, the structure is described with seven F non equivalent crystallographic sites, while in model 2, it is described with eight F sites (Table 1). The structure is built from a network of both opposite corner-sharing $Ga2F_6^{3-}$ octahedra forming infinite chains along the *c*-axis and isolated $Ga1F_6^{3-}$ octahedra. Three types of fluorine ions are encountered: shared fluorine, F3, that links two $Ga2F_6^{3-}$ octahedra; unshared fluorines, F1, F2, F4, F6, and F7 (model 1) or F7 and F8 (model 2), that belong to one GaF_6^{3-} octahedron; and "free" fluorine, F5, that does not belong to any GaF_6^{3-} octahedron. The Ga−F and F−Pb distances for both models are summarized in Tables 2 and 3, respectively. On one hand, model 1 leads to a particularly

(57) Massiot, D.; Fayon, F.; Capron, M.; King, I.; Le Calvé, S.; Alonso, B.; Durand, J. O.; Bujoli, B.; Gan, Z.; Hoatson, G. *Magn. Reson. Chem.* **2002**, *40*, 70–76.
(58) Willis, B. T. M.; Pryor, A. W. *Thermal Vibrations in Crystallography*; Cambridge University Press: London, 1975.

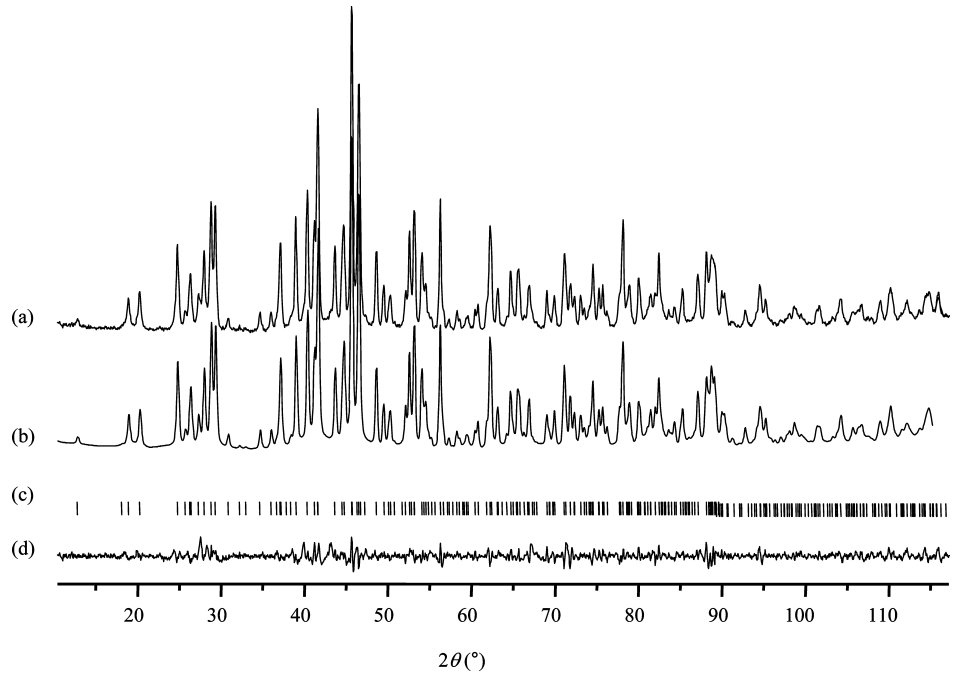

Figure 1. (a) Experimental and (b) calculated NPD diagrams of $Pb_5Ga_3F_{19}$ recorded at room temperature using model 1. (c) Vertical bars representing the Bragg positions. (d) Difference between experimental and calculated data.

short Ga2−F3 distance (1.762 Å) compared to the Ga−F distance in GaF_3[59] (1.885 Å) or to the sum of the ionic radii[60] (1.905 Å). On the other hand, model 2 gives a quite long Ga2−F3 distance (2.031 Å).

While Pb2 does not bond to F3 and F7 (or F7 and F8) as shown in Figure 4, Pb1 is affected strongly by the static disorder of the fluorine ions of the GaF_6^{3-} octahedron chains (Table 3). Depending on the position of the fluorine atoms of the $Ga2F_6^{3-}$ octahedra in model 2, the Pb1−F distances can vary drastically. For example, while the Pb1−F3 distance is unique and equal to 3.495 Å in model 1, different Pb1−F3 distances are possible in model 2, which range from 2.947 to 4.049 Å (Table 3). Similarly, the Pb1−F7 distances in model 1 vary from 2.718 to 2.986 Å, while in model 2 the Pb1−F7 or Pb1−F8 distances now vary over a much larger range (2.593−3.237 Å). Model 2 offers the advantage of allowing a quantification of the disorder of the Pb1 environment.

3. NMR Experiments. (i) ^{19}F NMR. The ^{19}F Hahn echo MAS spectrum of $Pb_5Ga_3F_{19}$ recorded with ^{207}Pb decoupling is shown in Figure 5. The spectrum exhibits particularly broad resonances (∼2 kHz) which arise from the structural disorder of this compound leading to distributions of the ^{19}F isotropic chemical shifts. This was supported by ^{19}F frequency-switched Lee−Goldburg (FSLG) homonuclear decoupling experiments which did not improve the resolution in the ^{19}F 1D MAS spectrum.[29] Eight lines are used to reconstruct the ^{19}F MAS NMR spectrum (Table 4): two with relative intensity of 2.3% (lines 1 and 2), three with relative intensity ranging from 8.1 to 10.1% (lines 3, 7, and 8), and three with relative intensity ranging from 21.5 to 24.1% (lines 4−6). One can notice that the ^{19}F NMR spectrum of $Pb_5Ga_3F_{19}$ shows an improved resolution compared to the spectrum recorded by Bureau et al.[46] at lower MAS frequency (in particular lines 1 and 2 were not resolved). As previously shown, free and shared fluorine ions have the highest and lowest isotropic chemical shifts, respectively,[46] while unshared fluorine ions stand between them. On the basis of these chemical shifts, line 8 (10.1%) is unambiguously assigned to the free fluorine ion, F5, which is still consistent with the expected relative line intensity (10.5%), and lines 1 and 2 are assigned to shared fluorine ions (expected relative line intensity of 5.3%). Model 1 for the structure of $Pb_5Ga_3F_{19}$ contains only one shared fluorine site, which exhibits a large ADP. The existence of the two shared fluorine resonances supports the static disorder of this position. Finally, the five remaining lines account for the unshared fluorine ions. The two ^{19}F resonances with relative intensities of 8.1 and 9.1% are assigned to F4 and F6 (expected intensity of 10.5%), and the three lines with the highest relative intensities (expected intensity of 21%) to F1, F2, and F7 (or F7 and F8, depending on the model). So far, a more accurate assignment of these lines is not possible.

(ii) ^{71}Ga NMR. The 17.6 T static and MAS ^{71}Ga NMR spectra, as well as the 9.4 T static ^{71}Ga spectrum of $Pb_5Ga_3F_{19}$, exhibit two lines with respective intensities of 32 and 68% (Figure 6). Regarding their relative intensities, line 1 is assigned to Ga2 and line 2 to Ga1. The ^{71}Ga isotropic chemical shifts of $Pb_5Ga_3F_{19}$ (Table 5) are typical of gallium in GaF_6^{3-} octahedra.[48,61] The quadrupolar parameters, determined from line shape simulation of the high-field static MAS and from the 9.4 T static ^{71}Ga NMR spectra (Figure 6), are gathered in Table 5. A unique set of parameters allows a good simulation of all the

(59) Roos, M.; Meyer, G. *Z. Kristallogr.−New Cryst. Struct.* **2001**, *216*, 18.
(60) Shannon, R. D. *Acta Crystallogr.* **1976**, *A32*, 751–767.
(61) Krahl, T.; Ahrens, M.; Scholz, G.; Heidemann, D.; Kemnitz, E. *Inorg. Chem.* **2008**, *47*, 663–670.

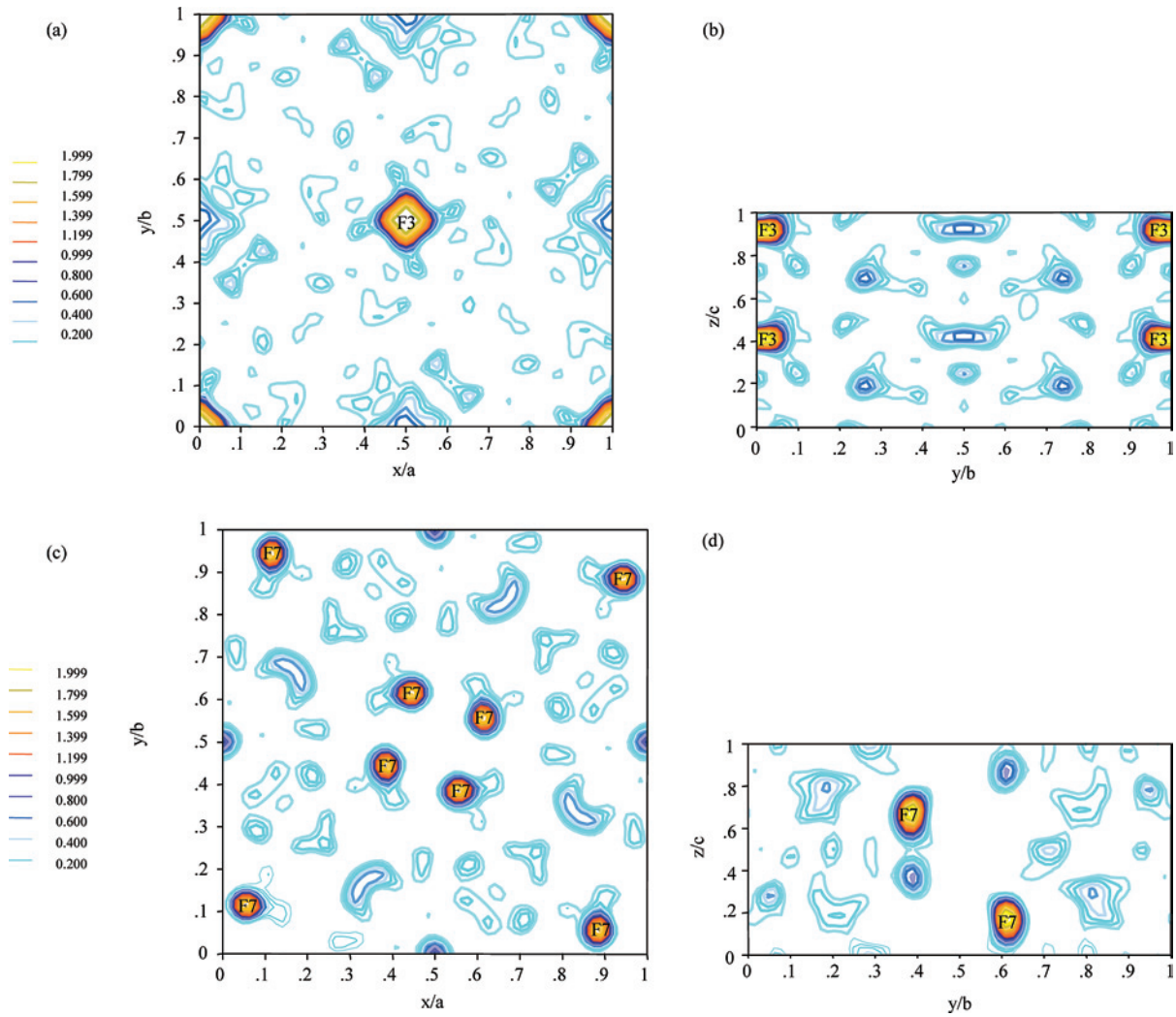

Figure 2. Fourier difference maps of $Pb_5Ga_3F_{19}$ calculated from model 1 without the F3 ion in the (a) $x-y$ plane at $z = 0.4063$ and (b) $y-z$ plane at $x = 0$ and without the F7 ion in the (c) $x-y$ plane at $z = 0.1875$ and (d) $y-z$ plane at $x = 0.4375$. The nuclear-scattering density scale is on the left. Missing atoms are labeled.

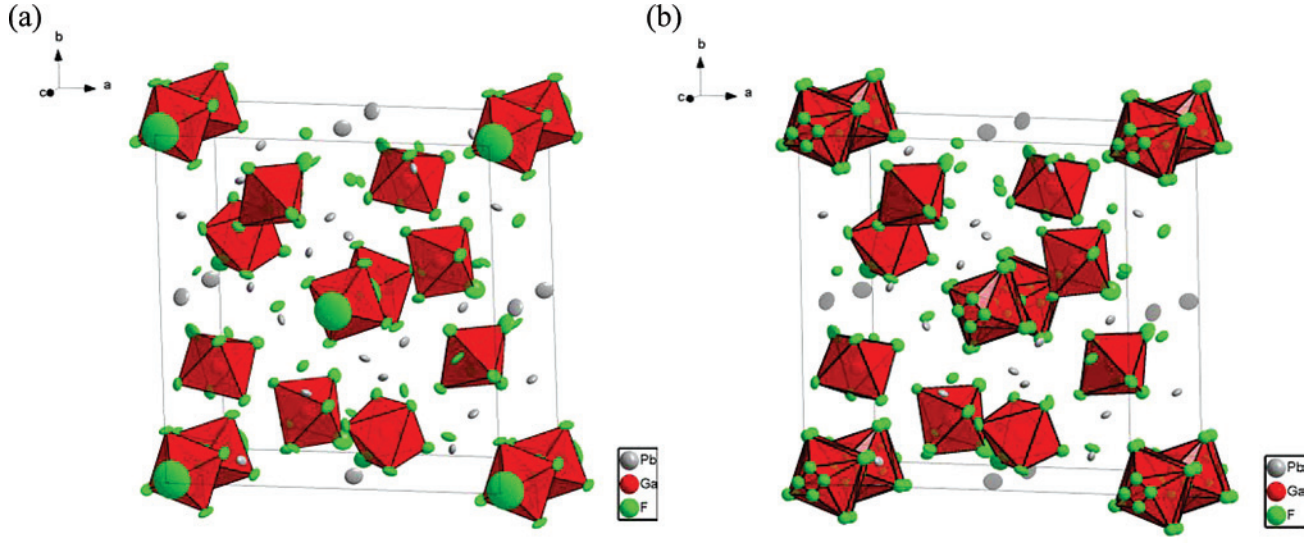

Figure 3. Perspective view of (a) model 1 and (b) model 2 of $Pb_5Ga_3F_{19}$. The GaF_6^{3-} octahedra with all the possible positions for F3, F7, and F8 in model 2 are shown. Thermal ellipsoids (50% probability) are represented.

spectra, which attests to its accuracy. It should be mentioned that the values of the ^{71}Ga parameters given in Table 5 are in agreement with the values reported for the Ga2 resonance by Bureau et al.[48] However, in that work carried out at a lower

Table 2. Ga−F Distances of Model 1 and Model 2 (in italic) of $Pb_5Ga_3F_{19}$

	distance (Å)		distance (Å)
Ga1−F4	1.845	Ga2−F3	1.762
	1.852		*1.860*
Ga1−F6	1.876	Ga2−F3	1.955
	1.869		*2.031*
Ga1−F1	1.912 (x2)	Ga2−F7	1.842 (x4)
	1.896 (x2)		*1.899 (x2)*
Ga1−F2	1.926 (x2)	Ga2−F8	*1.853 (x2)*
	1.931 (x2)		

Table 3. F−Pb Distances of < 3.5 Å for Model 1 and Model 2 (in italic) of $Pb_5Ga_3F_{19}$

atom		F−Pb distance (Å)	atom		F−Pb distance (Å)
F1	Pb1	2.456	F1	Pb1	*2.471*
	Pb1	2.897		Pb1	*2.891*
	Pb1	3.336		Pb1	*3.337*
F2	Pb1	2.547	F2	Pb1	*2.543*
	Pb1	2.796		Pb1	*2.792*
	Pb2	3.022		Pb2	*3.023*
F3	Pb1	3.495	F3	Pb1	*2.947*
	Pb1	3.495		Pb1	*3.424*
	Pb1	3.495	F4	Pb1	*2.595*
	Pb1	3.495		Pb1	*2.595*
F4	Pb1	2.591	F5	Pb1	*2.357*
	Pb1	2.591		Pb1	*2.357*
F5	Pb1	2.352		Pb2	*2.497*
	Pb1	2.352		Pb2	*2.406*
	Pb2	2.511	F6	Pb2	*2.417*
F6	Pb2	2.405		Pb1	*2.593*
	Pb2	2.413	F7	Pb1	*2.701*
F7	Pb1	2.718		Pb1	*3.237*
	Pb1	2.828		Pb1	*2.739*
	Pb1	2.986	F8	Pb1	*2.850*
				Pb1	*2.983*

magnetic field (7 T), the Ga1 resonance was simulated with two slightly different contributions, possibly because of a significantly lower resolution of the ^{71}Ga static spectrum. The Ga2 resonance exhibits a very large quadrupolar coupling constant (Table 5). As observed for the AlF_6^{3-} octahedra in fluoroaluminates,[62,63] the gallium ions of the $Ga2F_6^{3-}$ octahedra, which contain both unshared and shared fluorine ions, have a ν_Q value higher than that of the gallium ions of the isolated $Ga1F_6^{3-}$ octahedra. Ga2 has an asymmetry parameter, $\eta_Q = 0$, that is in agreement with the location of Ga2 on a four-symmetry axis. This unique set of quadrupolar parameter values accounts for identical rigid $Ga2F_6^{3-}$ octahedra, retaining locally the 4-fold axial symmetry. Thus, the disorder of the fluorine sites belonging to these octahedra indicates a disorder of the orientation of the rigid $Ga2F_6^{3-}$ octahedra within the chains. In a given chain, $Ga2F_6^{3-}$ octahedron tilts lead to occupancy of only two of the four possible shared fluorine sites (F3) of model 2. This should imply several unshared fluorine positions above, below, and in the equatorial plane parallel to the $a-b$ plane as defined in model 1 (Figure 7). This assumption is not fully described in model 2. One may outline that whatever method used to split the disordered fluorine sites it seems unlikely that any crystallographic model could give adjacent F−Ga2−F angles equal to 90°, which are imposed by the 4-fold axial symmetry of the $Ga2F_6^{3-}$ octahedra and clearly shown by NMR. The example of $Pb_5Ga_3F_{19}$ illustrates the difficulty of fully describing the structure of crystalline but disordered compounds when building crystallographic models from diffraction data only.

(iii) ^{207}Pb NMR. The ^{19}F decoupled ^{19}F−^{207}Pb CP-MAS and *J*-INEPT spectra of $Pb_5Ga_3F_{19}$ are displayed in Figure 8. Similar to the ^{19}F spectrum, the ^{207}Pb resonances are broad, partly due to the structural disorder of the compound that induces chemical shift distributions. Comparison of the spectra recorded at various MAS frequencies allows distinction of four isotropic resonances (Figure 8 and Table 6). One can notice that lines 1, 3, and 4 are much broader (7−10 kHz) than line 2 (~3 kHz). Relative intensities of lines 1, 3, and 4 vary with the spinning speed and the nature of the transfer (dipolar or scalar), which complicates the line assignment. However, for all spectra, line 2 has a relative intensity of ~20% of the total signal. In addition, this line is significantly narrower than the other lines. For these reasons, it is assigned to Pb2, whose environment is not affected by the static disorder of the fluorine ions of the $Ga2F_6^{3-}$ octahedra. The three remaining resonances finally correspond to the signal of the Pb1 crystallographic site (80% of the total lead atoms). It should be mentioned that the signal of the Pb1 site was not clearly detected by Bureau et al.,[47] mostly because of their large broadening and strong temperature dependence. Considering the well-known high sensitivity of the ^{207}Pb chemical shift to its environment,[51] the large range of the ^{207}Pb isotropic chemical shift associated with the signal of the Pb1 site (~500 ppm) is due to the disorder of the fluorine ions of the $Ga2F_6^{3-}$ octahedra. Because of large ADP values for the F3 and F7 sites, model 1 should give a unique but particularly broad resonance. The three broad but discrete ^{207}Pb lines experimentally observed are related to different Pb1−F distances, which may be expected from model 2 (Table 3).

So far, the 1D ^{19}F, ^{71}Ga, and ^{207}Pb NMR results are in agreement with a static disorder of the fluorine ions of the $Ga2F_6^{3-}$ octahedron chains. This disorder cannot be described simply by a crystallographic model issued from diffraction data. To check if both models can correctly describe the medium-range order of the structure of $Pb_5Ga_3F_{19}$, homonuclear (^{19}F−^{19}F) and heteronuclear (^{19}F−^{207}Pb) 2D NMR correlation experiments were carried out and are presented in the following sections.

(iv) ^{19}F−^{19}F Homonuclear Correlations. Two-dimensional ^{19}F homonuclear DQ-SQ MAS NMR experiments, based on through-space ^{19}F−^{19}F dipolar coupling (directly related to the F−F distances), can be used to help assignment of the ^{19}F resonances.[30] In 2D ^{19}F DQ-SQ MAS NMR correlation spectra, the fluorine atomic proximities are revealed by paired cross-correlation peaks, which appear at the individual chemical shifts of the two dipolar-coupled nuclei in the SQ dimension and at the sum of these chemical shifts in the DQ dimension. Autocorrelation peaks are produced only if ^{19}F environments with identical chemical shifts are dipolar coupled. In homonuclear spin systems of

(62) Body, M.; Legein, C.; Buzaré, J.-Y.; Silly, G. *Eur. J. Inorg. Chem.* **2007**, 1980–1988.
(63) Body, M.; Legein, C.; Buzaré, J.-Y.; Silly, G.; Blaha, P.; Martineau, C.; Calvayrac, F. *J. Phys. Chem. A* **2007**, *111*, 11873–11884.

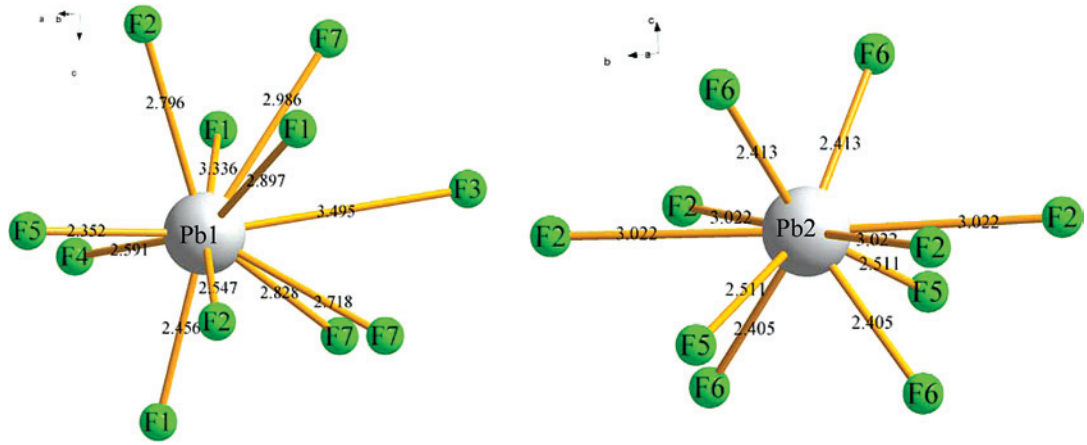

Figure 4. Representation of the $Pb1F_{11}$ polyhedron (left) and the $Pb2F_{10}$ polyhedron (right) of model 1 of $Pb_5Ga_3F_{19}$. Pb−F distances are given in angstroms.

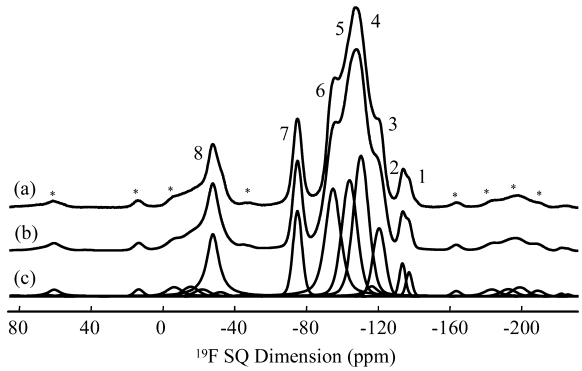

Figure 5. (a) Experimental and (b) calculated ^{19}F MAS (25 kHz) Hahn echo spectra of $Pb_5Ga_3F_{19}$. Stars indicate spinning sidebands. Eight individual contributions are shown in (c).

Table 4. ^{19}F Line Label, Isotropic Chemical Shift δ_{iso}, Relative Intensity, Initial Assignment,[a] Final Assignment, and $^{19}F-^{207}Pb$ *J*-Coupling Constant Value in $Pb_5Ga_3F_{19}$

line	δ_{iso} (±1) (ppm)	intensity (±0.5) (%)	initial	final	J^{29} (kHz)
1	−137	2.3	F3	F3	0.9
2	−133	2.3	F3	F3	0.9
3	−119	9.1	F4 or F6	F4	1.9
4	−110	21.5	F1 or F2 or F7 and F8	F1	1.5
5	−105	22.1	F1 or F2 or F7 and F8	F7 and F8	1.9
6	−96	24.1	F1 or F2 or F7 and F8	F2	1.5
7	−75	8.1	F4 or F6	F6	4.6 and 2.1
8	−28	10.1	F5	F5	2.0

[a] Deduced from intensity and δ_{iso} values.

abundant nuclei (like to ^{19}F), the DQ-SQ correlation spectra are dominated by the strongest couplings because of dipolar truncation,[64−66] where the polarization transfer across a weak dipolar coupling is quenched by the simultaneous presence of a larger dipolar coupling. In our case, we experimentally observe that only ^{19}F dipolar couplings larger than 2.1 kHz (corresponding to $^{19}F-^{19}F$ distances less than 3.7 Å) give rise to correlation peaks with significant intensities in the 2D DQ-SQ MAS correlation spectrum.

(64) Hohwy, M.; Rienstra, C. M.; Jaroniec, C. P.; Griffin, R. G. *J. Chem. Phys.* **1999**, *110*, 7983–7992.
(65) Hohwy, M.; Rienstra, C. M.; Griffin, R. G. *J. Chem. Phys.* **2002**, *117*, 4973–4987.
(66) Grommek, A.; Meier, B. H.; Ernst, M. *Chem. Phys. Lett.* **2006**, *427*, 404–409.

As previously described, the structure of $Pb_5Ga_3F_{19}$ is built from GaF_6^{3-} octahedra. Therefore, strong dipolar couplings between two adjacent fluorine ions, and significantly weaker dipolar interactions between two opposite fluorine ions are expected (Figure 9a). Fluorine ions belonging to different octahedra can also be detected provided that sufficiently short F−F distances exist. The ^{19}F DQ-SQ MAS spectrum of $Pb_5Ga_3F_{19}$ recorded with ^{207}Pb decoupling in both dimensions is shown in Figure 9b. The ^{19}F chemical shift range of $Pb_5Ga_3F_{19}$ is too large to allow rotor synchronization in the DQ dimension. Thus, a part of the spectrum is folded, which does not prevent correlation determination. It should be noted that the recoupling efficiency of the BABA sequence employed here is known to be sensitive to the offset. In particular, weak recoupling efficiency is expected for the resonances of the free fluorine ion, which is far from the carrier frequency and for which correlation peaks of very weak intensities were experimentally observed (below the contour levels plotted in Figure 9b). Finally, the ^{19}F DQ-SQ spectrum of $Pb_5Ga_3F_{19}$ shows that lines 1 and 2, which correspond to the shared fluorine ion F3, are strongly coupled to line 5 (intensity of 22.1% in the ^{19}F MAS spectrum). Therefore, line 5 is assigned to the unshared fluorine ions of the $Ga2F_6^{3-}$ infinite chains, F7 (or F7 and F8), which are the closest fluorine neighbors of F3 (Table 7). F3 is also weakly coupled to line 4, which is then assigned to F1. Opposite F4 (line 3) and F6 (line 7) of $Ga1F_6^{3-}$ are not coupled to each other but are both coupled to F1 (line 4) and F2 (line 6) as shown in Figure 9b and reported in Table 7. Two adjacent F1 and two adjacent F2 form an equatorial plane of the isolated $Ga1F_6^{3-}$ octahedron (Figure 3), which is observed on the ^{19}F DQ-SQ MAS spectrum by diagonal correlation peaks. Correlations between fluorine ions belonging to different octahedra are observed, for example, between F7 (or F7 and F8) from the $Ga2F_6^{3-}$ octahedron (line 5) and F4 from the $Ga1F_6^{3-}$ octahedron (line 3). This DQ-SQ correlation spectrum allows complete assignment of the ^{19}F MAS resonances of $Pb_5Ga_3F_{19}$ (Tables 4 and 7), which is in full agreement with the reported structural models.

(v) $^{19}F-^{207}Pb$ Heteronuclear Correlations. The 2D $^{19}F-^{207}Pb$ *J*-HMQC spectrum of $Pb_5Ga_3F_{19}$ shows that the

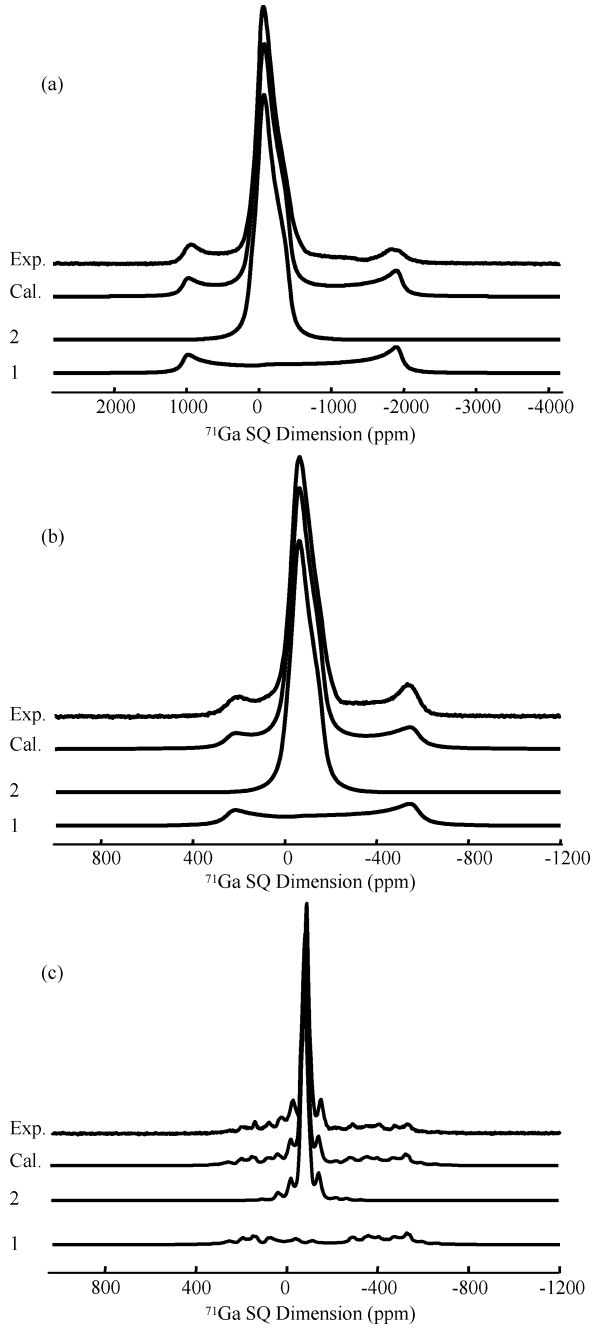

Figure 6. Experimental and calculated ^{71}Ga Hahn echo spectra of $Pb_5Ga_3F_{19}$: (a) static recorded at 9.4 T, (b) static recorded at 17.6 T, and (c) MAS (14 kHz) recorded at 17.6 T. Individual components, as labeled in Table 5, are shown.

Table 5. ^{71}Ga Line Label, Isotropic Chemical Shift δ_{iso}, Relative Intensity, Quadupolar Coupling Constant C_Q, Quadrupolar Frequency ν_Q, Asymmetry Parameter η_Q, and Assignment[a] of $Pb_5Ga_3F_{19}$

line	δ_{iso} (±1) (ppm)	intensity (±2) (%)	C_Q (±0.05) (MHz)	ν_Q[b] (±10) (kHz)	η_Q (±0.1)	assignment
1	−53	32	18.20	9100	0	Ga2
2	−56	68	5.68	2840	0.85	Ga1

[a] Deduced from the reconstruction of the ^{71}Ga NMR spectra. [b] The relation between ν_Q and C_Q is $\nu_Q = 3C_Q/[2I(2I-1)]$.

Pb1−F correlation pattern is repeated for each Pb1 resonance, which supports the assignment of these resonances to the same Pb1 lead site (Figure 10a). Lines 3 and 7 (relative intensity of 10.5% in the ^{19}F MAS spectrum) are correlated

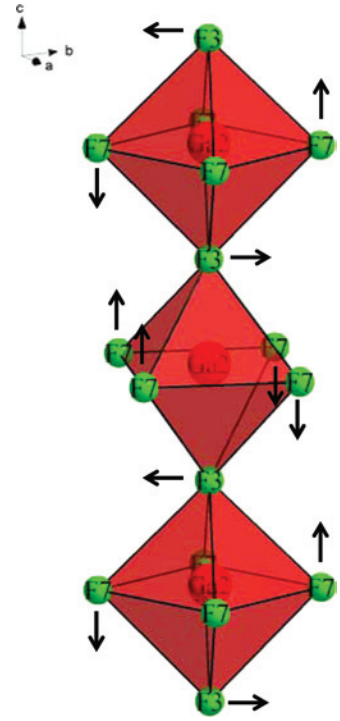

Figure 7. Representation of $Ga2F_6^{3-}$ octahedra in $Pb_5Ga_3F_{19}$ (model 1). Atoms are labeled. Arrows indicate possible directions of the octahedra tilt.

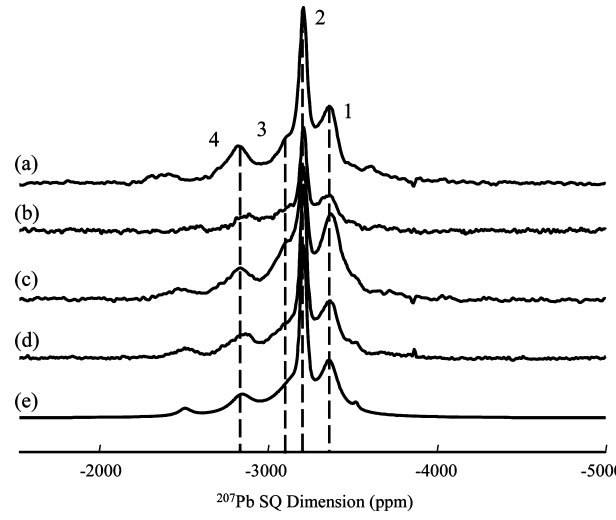

Figure 8. (a, c) Experimental MAS ^{19}F−^{207}Pb *J*-INEPT spectra and (b, d) CP spectra of $Pb_5Ga_3F_{19}$ recorded at a spinning speed of 25 kHz (a, b) and 20 kHz (c, d). The reconstruction of the CP-MAS (20 kHz) is shown in (e). Dashed lines indicate the isotropic positions. Non labeled peaks are spinning sidebands.

Table 6. ^{207}Pb Line Label, Isotropic Chemical Shift δ_{iso}, and Assignment[a] of $Pb_5Ga_3F_{19}$

line	δ_{iso} (±5) (ppm)	assignment
1	−3370	Pb1
2	−3210	Pb2
3	−3110	Pb1
4	−2840	Pb1

[a] Deduced from the reconstruction of the ^{207}Pb NMR spectra.

to Pb1 and Pb2, respectively (Figure 10). This unambiguously confirms their assignment to F4 and F6, respectively, which was previously deduced from the ^{19}F DQ-SQ spectrum, because F4 has only Pb1 atom neighbors, whereas F6

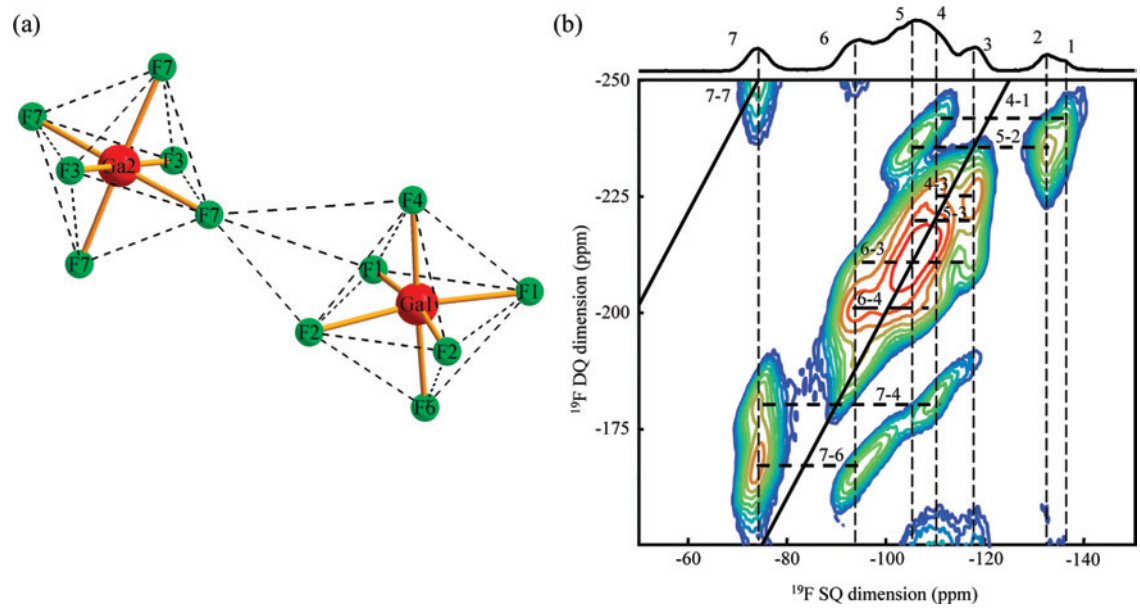

Figure 9. (a) Representation of GaF_6^{3-} octahedra (model 1) in $Pb_5Ga_3F_{19}$. Dashed lines indicate fluorine−fluorine proximities giving rise to observable peaks on the DQ-SQ spectrum. (b) ^{19}F DQ-SQ MAS (30 kHz) spectrum of $Pb_5Ga_3F_{19}$ recorded using a BABA recoupling sequence. The single quantum projection is shown on top, where ^{19}F lines are labeled. Vertical dashed lines indicate ^{19}F line positions. Thick solid lines indicate the diagonal of the spectrum on which autocorrelation peaks appear. Horizontal dashed lines indicate selected fluorine−fluorine correlations. An exhaustive list of $^{19}F-^{19}F$ correlations is given in Table 7.

Table 7. ^{19}F Line Label, Line Assignment, $^{19}F-^{19}F$ Line Correlations, and F Atom Neighbors to F Atoms[a] in Models 1 and 2 (in italic) of $Pb_5Ga_3F_{19}$[b]

line	assignment	$^{19}F-^{19}F$ line correlations	F neighbors
1	F3	4,5	F7
			F8, F7, F1
2	F3	4,5	F7
			F8, F7, F1
3	F4	4,5,6	F1, F5, F2
			F1, F5, F2, F7, F8
4	F1	1,2,3,4,5,6,7	F2, F6, F4, F1, F7, F5
			F2, F6, F4, F8, F1, F7, F5, F3
5	F7	1,2,3,4,5,6	F3, F7, F2, F1
	F7 and F8		*F3, F7, F2, F8, F1, F4 F3,*
			F8, F7, F2, F1, F4
6	F2	3,4,5,6,7	F6, F2, F1, F7, F4, F5
			F6, F1, F2, F7, F8, F4, F5
7	F6	4,6,7	F2, F1, F5, F6
			F2, F1, F5, F6
8	F5	/	F4, F6, F2, F1
			F4, F6, F2, F1

[a] F−F distances less than 3.6 Å. [b] F atoms are listed in order of increasing F−F distances.

has only Pb2 as first neighbors (Table 3). F5, the free fluorine ion, is correlated to both Pb1 and Pb2 as expected from the crystallographic models. The correlation peak between F3 and Pb1 is too small to be detected. From the ^{19}F DQ-SQ MAS spectrum, line 5 was assigned to F7 (or F7 and F8). As expected, they are correlated only to Pb1 in the *J*-HMQC spectrum. Finally, lines 4 and 6 are unambiguously assigned to F1 and F2, respectively (Table 4), as F1 only shows a correlation peak with the Pb1 resonance, whereas F2 is linked to both Pb1 and Pb2 (Table 3). This also confirms the assignment deduced from the ^{19}F DQ-SQ MAS spectrum. In addition, fluorine−lead correlations are also observed on a $^{19}F-^{207}Pb$ CP-HETCOR spectrum (Figure 10), in spite of the lower resolution in the indirect ^{19}F dimension. Cross-correlations do not have the same intensities as in the *J*-HMQC spectrum. This is expected because correlation peak intensities in the *J*-HMQC experiment depend on both the $^{19}F-^{207}Pb$ scalar coupling value and the ^{19}F transverse dephasing time, while correlation peak intensities in the HETCOR experiment are mainly affected by the $^{19}F-^{207}Pb$ dipolar couplings and spin-lock efficiency (RF field strength, offset, chemical shift anisotropy, and longitudinal relaxation rate in the rotating frame). Similar to the *J*-HMQC spectrum, the Pb1−F correlation pattern is spread over the three Pb1 resonances. Despite a long experimental time for the CP-HETCOR sequence (3 days), the low resolution of the CP-HETCOR spectrum prevents the complete ^{19}F NMR line assignment. This highlights the efficiency of the *J*-HMQC experiment, which allows the unambiguous assignment of the ^{19}F MAS resonances to all the inequivalent fluorine crystallographic sites within an experimental time of only 4 h.

The ^{19}F and ^{207}Pb NMR spectrum assignments allow a possible relationship between the $^{19}F-^{207}Pb$ *J*-coupling constant values,[29] the fluorine sites, and the environments to be investigated in $Pb_5Ga_3F_{19}$ (Table 4). Nevertheless, in this disordered compound, despite the structure determination a straightforward empirical relationship between $^{19}F-^{207}Pb$ *J*-coupling constant values and Pb−F distances could not be established.

Conclusions

The room temperature structure of $Pb_5Ga_3F_{19}$ is investigated by combining neutron diffraction and multinuclear 1D and 2D NMR experiments on powder samples. Two models built in SG *I*4*cm* are reported for the description of the crystalline structure of $Pb_5Ga_3F_{19}$. The two models offer two slightly different views of the strong static disorder of the fluorine ions belonging to the $Ga2F_6^{3-}$ octahedra forming

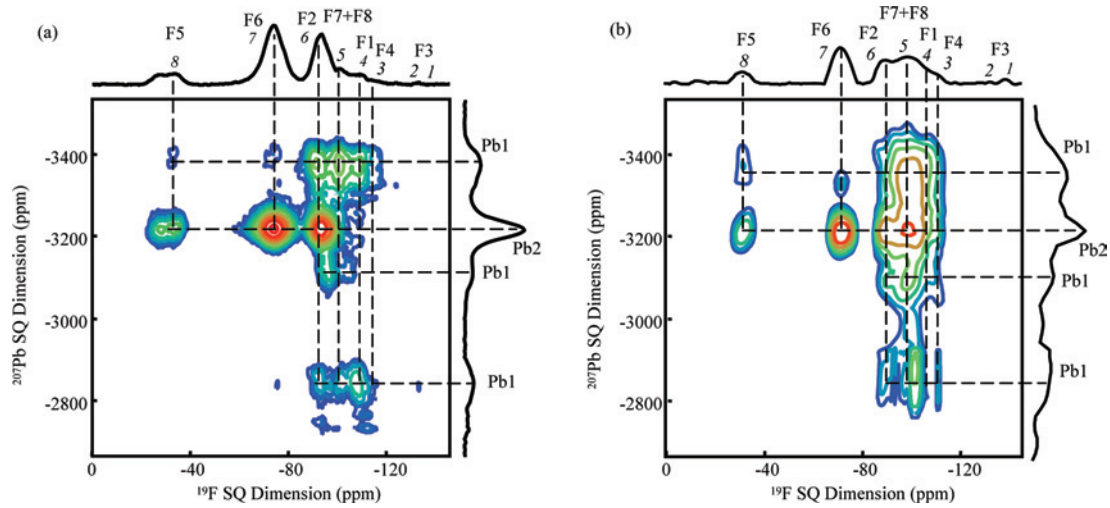

Figure 10. (a) $^{19}F-^{207}Pb$ MAS (25 kHz) *J*-HMQC spectra and (b) $^{19}F-^{207}Pb$ CP-HETCOR spectra of $Pb_5Ga_3F_{19}$. Dashed lines indicate $^{19}F-^{207}Pb$ correlations. Single quantum projections of ^{19}F (with line labels in italic and line assignments) and ^{207}Pb (with line assignments) are shown on the top and to the right, respectively.

infinite chains along the *c*-axis. ^{71}Ga NMR results show that the local environment of all Ga2 ions is identical, which reflects a tilt of the $Ga2F_6^{3-}$ octahedra within the chains. ^{207}Pb NMR experiments confirm that the environment of only one of the two lead sites, Pb1, is strongly affected by the disorder, which gives rise to three distinct ^{207}Pb NMR lines for this site. All ^{19}F NMR lines are assigned using the ^{19}F DQ-SQ MAS experiment. $^{19}F-^{207}Pb$ through-bond and through-space heteronuclear correlation experiments are carried out for the first time, supporting assignment of both the ^{19}F and ^{207}Pb NMR spectra. These correlation experiments also show that both models correctly describe the medium-range order of the structure of $Pb_5Ga_3F_{19}$. This study clearly illustrates the complementarities of both diffraction and NMR techniques and highlights the potential of 2D MAS NMR experiments for the characterization of inorganic fluorides.

Acknowledgment. C.M., C.L., and J.-Y.B. thank Gilles Silly from Institut Charles Gerhardt, UMR CNRS 5253, Université de Montpellier II, France, for having initiated this work when he was in Le Mans.

Supporting Information Available: CIF files of the two structural models of $Pb_5Ga_3F_{19}$. This material is available free of charge via the Internet at http://pubs.acs.org.

IC801044J